Electronic Supplementary Information (ESI)

A classical $[V_{10}O_{28}]^{6-}$ anion templated high-nuclearity silver thiolate cluster

Experimental details

The $\{(HNEt_3)_2[Ag_{10}(^tBuPhS)_{12}]\}_n$ precursor and H_4TC4A ligand were synthesized according to the relevant literatures.[1,2] The chemicals and solvents used in the syntheses were of analytical grade without further purification. The IR spectra were recorded on the Bruker Tensor II spectrophotometer (Bruker Optics GmbH, Ettlingen, Germany) employing a single attenuated total reflectance (ATR) accessory with a wavenumber range of 4000-500 cm^{-1}. The PXRD data were acquired by using a Rigaku Oxford Diffraction XtaLAB Synergy diffractometer with Cu radiation (λ = 1.54184 Å). The Powder function of the *CrysAlis^{Pro}* software suite[3] was used to process the PXRD patterns. UV-Vis diffuse reflectance spectrum was carried out on a Thermo Scientific Evolution 220 UV-visible spectrophotometer equipped with an 60 mm integrating sphere and SPECTRALON® was used as the reference. The optical band gap is determined based on the Kubelka-Munk function of $(\alpha h\upsilon)^{1/2} = \kappa(h\upsilon - E_g)$ (E_g is the band gap (eV), h is the Planck's constant (J.s), υ is the light frequency (s^{-1}), κ is the absorption constant and α is the absorption coefficient).[4,5] The ESI-MS was performed on a Bruker impact II high definition mass spectrometer, quadrupole and time-of-flight (Q/TOF) modules (end plate offset = -400 V; dry gas = 3 L min^{-1}; nebulizer = 0.3 bar; capillary voltage = 3500 V; sample flow rate = 180 μL h^{-1}). The data of ESI-MS was analyzed using Compass Data Analysis software (Version 4.4) based on the isotope distribution patterns. Photocurrent test and Mott-Schottky experiment were carried out on a CHI660E electrochemistry workstation. The crystals (3 mg) of **Ag50** and naphthol (0.5 wt.%, 10 μL) were dispersed in 0.3 mL ethanol, and then transferred by pipet to the cleaned ITO glass. The coated film used as working electrode was obtained after evaporation under ambient atmosphere. Differential scanning calorimetry and thermogravimetric analysis (DSC/TGA) measurement was performed with a TA SDT Q600 thermal analyzer at a scanning rate of 20 °C/min under N_2, from 20 to 800 °C.

X-ray crystallography

Fresh crystal of **Ag50** with high quality was picked out under an optical microscope and quickly wrapped with high vacuum grease (Dow Corning Corporation) to prevent decomposition. The SCXRD data was recorded on a Rigaku Oxford Diffraction XtaLAB Synergy diffractometer equipped with Rigaku Hypix detector at 100 K. Using a Cu Kα radiation (λ = 1.54184 Å) from PhotonJet micro-focus X-ray sources to measure. The diffraction images of **Ag50** were processed and scaled using the *CrysAlis*^{Pro} software.[3] Analytical numeric absorption correction was applied using a multifaceted crystal model based on expressions derived by R.C. Clark & J.S. Reid[6]. The structure was solved using SHELXT structure solution program[7] and refined by full-matrix least-squares techniques against F_o^2 using the SHELXL program[8] through the OLEX2 interface.[9] Hydrogen atoms at carbon were placed in calculated positions and refined isotropically by using a riding model. Appropriate restraints or constraints were applied to the geometry and the atomic displacement parameters of the atoms in the cluster. All structures were examined using the Addsym subroutine of PLATON[10] to ensure that no additional symmetry could be applied to the models. Pertinent crystallographic data collection and refinement parameters are collated in Table S4. Selected bond lengths and angles are collated in Table S5.

A solvent mask was calculated and 652.2 electrons were found in a volume of 2510.8 Å^3 void per formula unit. This is consistent with the presence of 4 CF_3COO^- and 10 DMF per formula unit which account for 624 electrons per formula unit.

Synthesis Details

The Ag_{50} cluster was synthesized using the combination of room temperature stirring and solvothermal method. Specifically, a mixture of $\{(HNEt_3)_2[Ag_{10}(^tBuPhS)_{12}]\}_n$ (13.7 mg, 0.05 mmol), H_4TC4A (10.8 mg, 0.015 mmol) and Na_3VO_4 (8 mg, 0.04 mmol) were immersed in 1 mL DMF and stirred magnetically for three hours at room temperature. Then, to the above mixture 0.5 mL DMF solution of CF_3COOAg (22.1 mg, 0.1 mmol) was added. The reaction proceeded for another three hours. Then, the brown turbid solution is sealed into a 25 mL teflon-lined autoclave and kept at 65 °C for 2000 minutes. After cooling to room temperature, black rod-like crystals of **Ag50** were deposited on the bottom of the bottle with a yield of ~21.5%. Repeated experiments were carried out in multiple batches under the same synthesis conditions, which confirmed the excellent reproducibility of the **Ag50** sample. After removing the H_4TC4A ligand from the synthesis procedure, the yield was less than 1%. Selected IR peaks (cm^{-1}): 2957 (m), 1647 (s), 1488 (m), 1395 (w), 1362 (w), 1275 (w), 1192 (s), 1149 (m), 1000 (m), 918 (m), 820 (m), 721 (s), 546 (s).

Figure S1: The crystal packing diagrams of **Ag50** in a unit cell viewed along *a*(a), *b*(b) and *c*(c) axis. Color code: purple, Ag; red, O; yellow, S; gray, C; green, F; blue, V; orange, N. The blue polyhedra represent $[V_{10}O_{28}]^{6-}$ template.

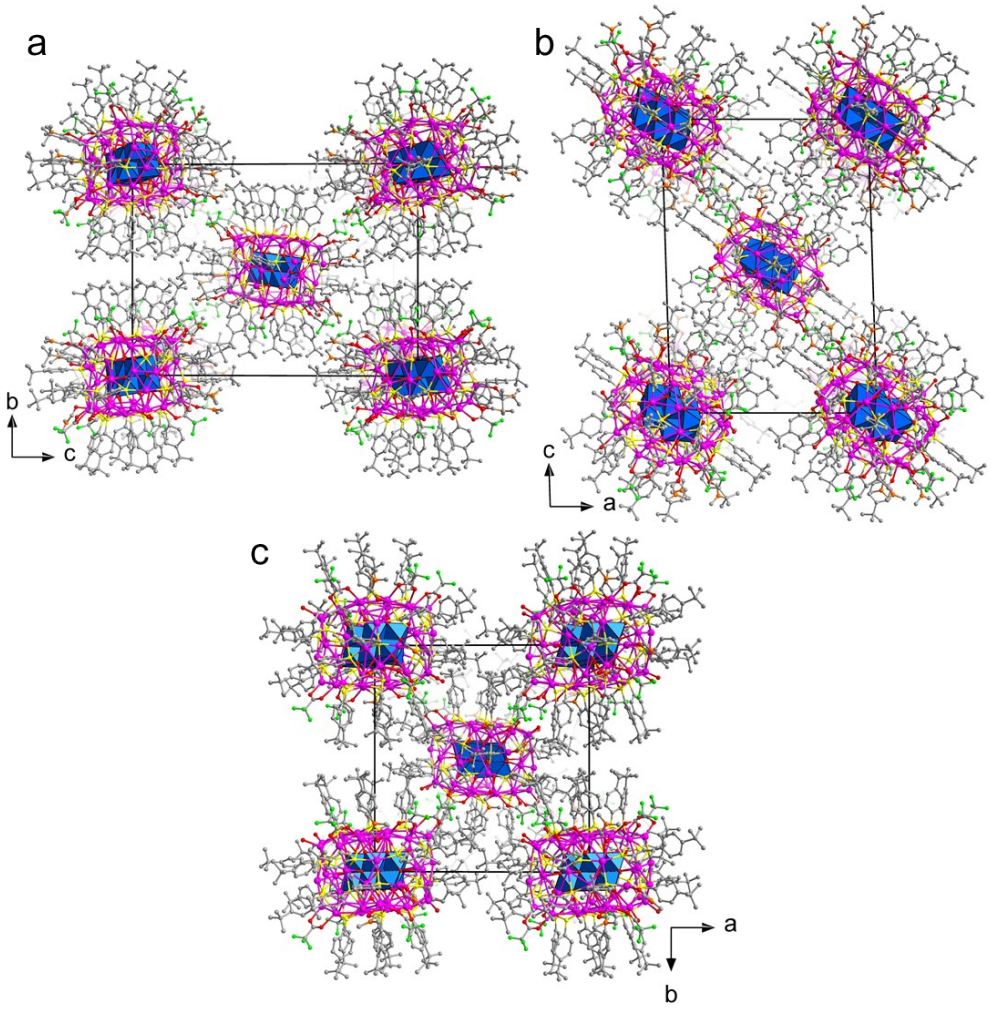

Figure S2: DSC/TGA curves of **Ag50** (heating rate 20 °C min^{-1}).

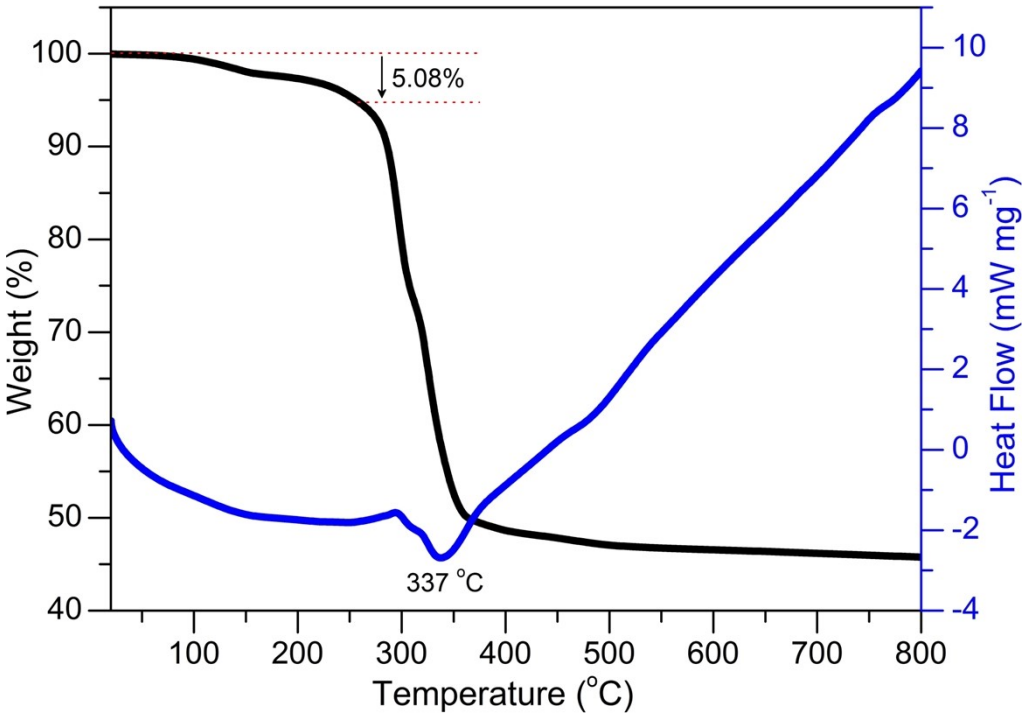

The TGA of the **Ag50** showed that a slight weight loss of 5.08% was found in the temperature range of 20-256 °C, which could be assigned to the loss of ten DMF molecules (calcd. 5.07%). The subsequent second major weight loss could be attributed to the decomposition of **Ag50** (256-367 °C), which is consistent with the endothermic peak of DSC curve at 337 °C.

Figure S3: (a) and (b) The $[V_{10}O_{28}]^{6-}$ template caged in box-like Ag_{50} shell viewed along two different directions. The inner polyhedra represent $[V_{10}O_{28}]^{6-}$ template.

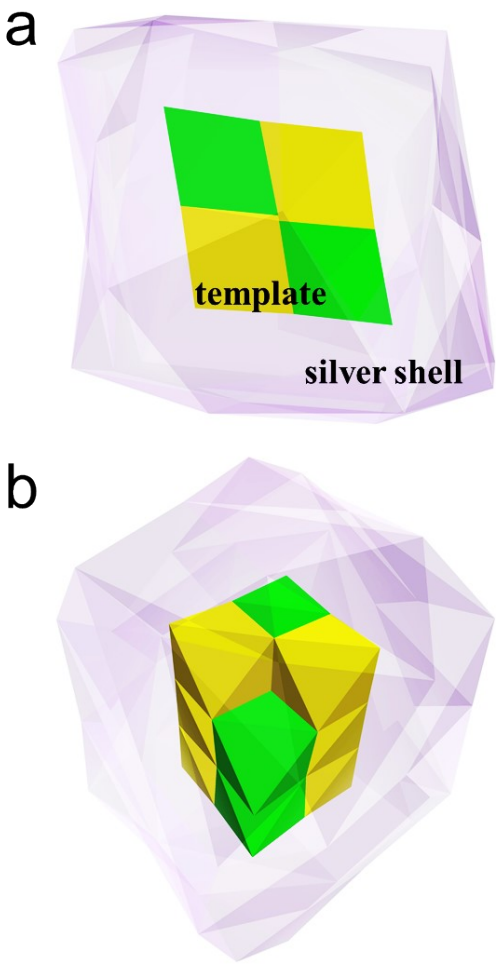

Figure S4: (a) and (b) One 2-fold axis passing through two silver atoms (cyan balls) of the Ag_{50} shell and four oxygen atoms (black balls) within the $[V_{10}O_{28}]^{6-}$ anion, viewed along two orthogonal directions. Color code: purple and cyan, Ag; red and black, O; yellow, S; gray, C; green, F; blue, V; orange, N.

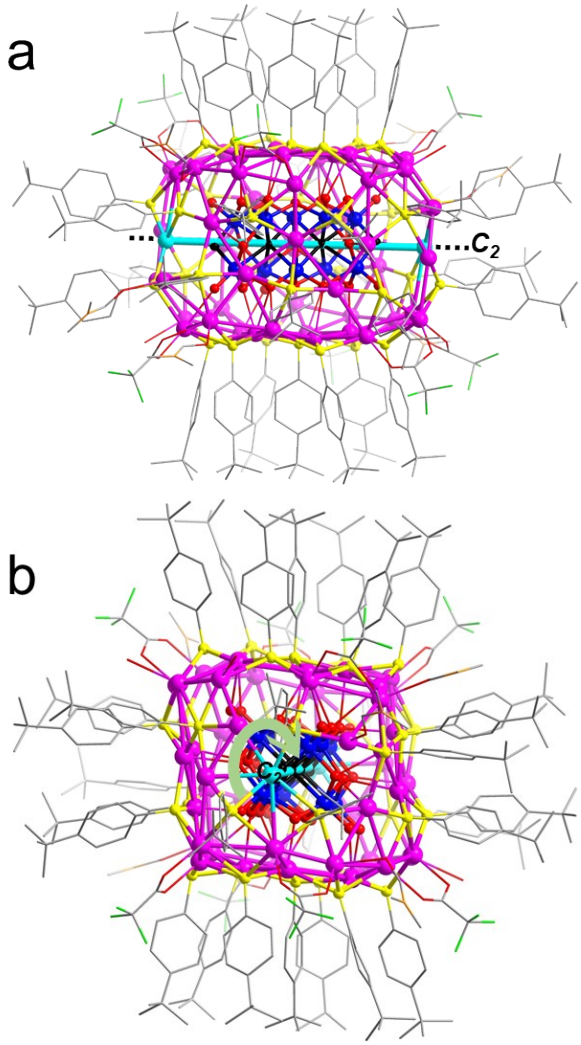

Figure S5: (a) and (b) The coordination modes of $[V_{10}O_{28}]^{6-}$ anion towards 24 silver atoms viewed along two orthogonal directions. Color code: purple, Ag; red, O; blue, V.

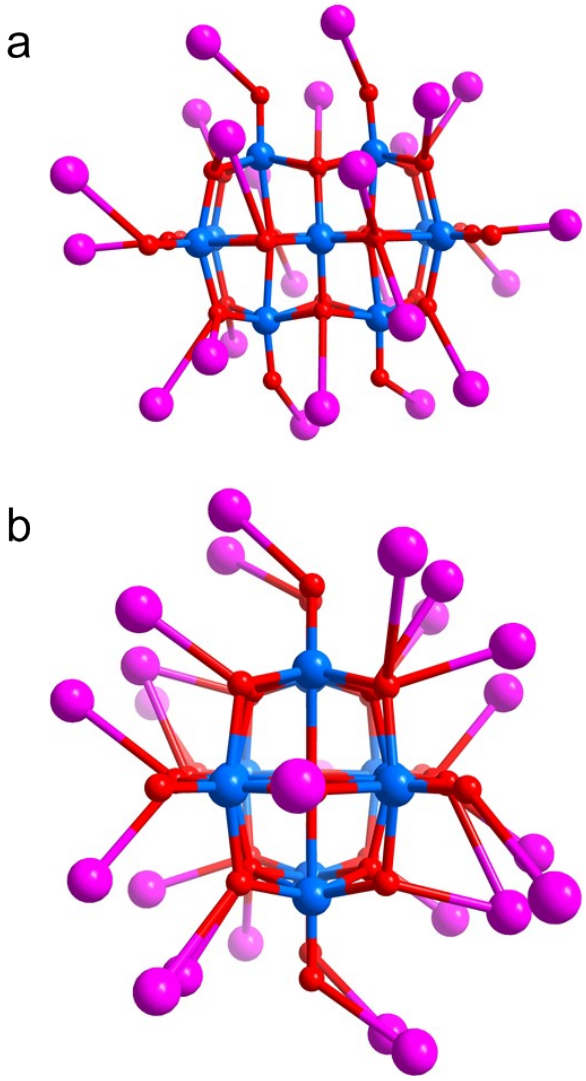

Figure S6: The arrangements of ^{t}BuPhS^{-} ligands on the surface of Ag_{50} shell. Color code: purple, Ag; yellow, S; gray, C.

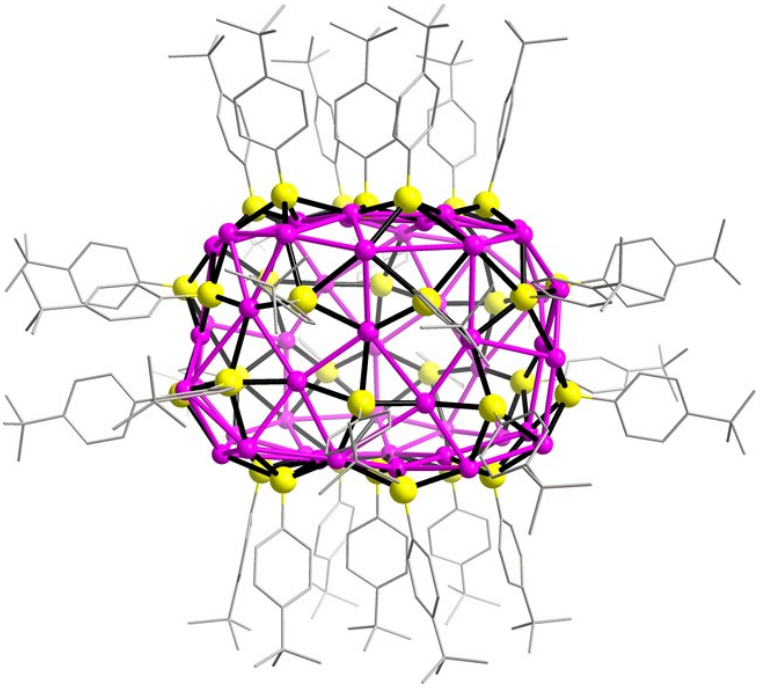

Figure S7: (a) and (b) Four-layered distribution of ^{t}BuPhS^{-} ligands marked in different colors viewed along two orthogonal directions. The ^{t}BuPhS^{-} ligand layers distributed from box cover to box body to opposite box cover are shown in pink, blue, yellow and green atoms, respectively.

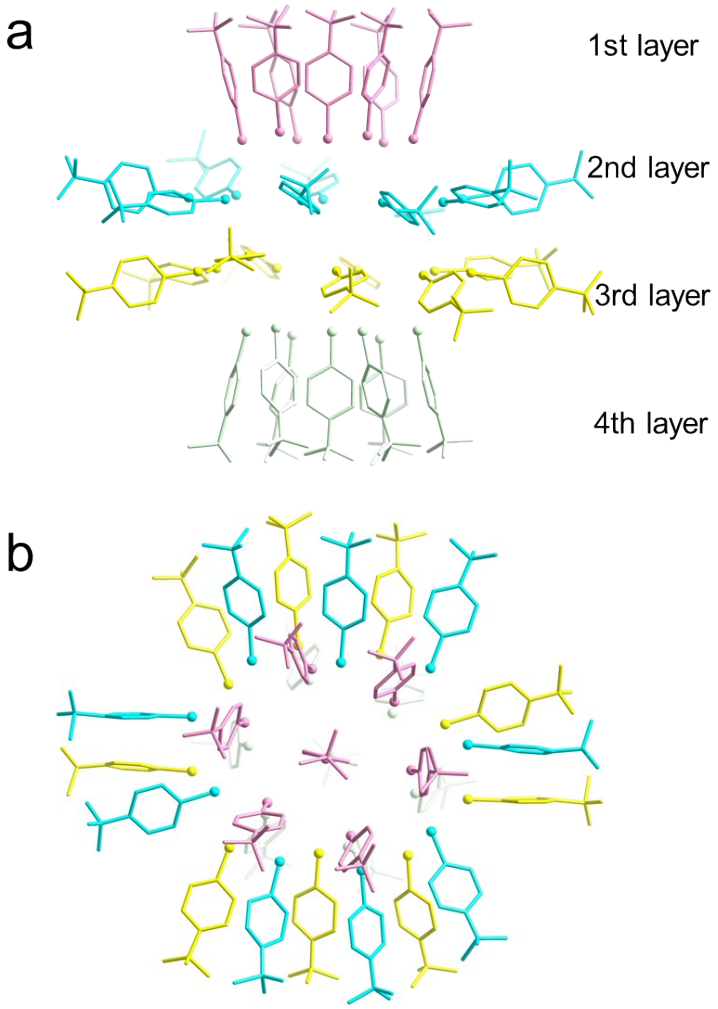

Figure S8: The arrangements of CF_3COO^- ligands on the surface of Ag_{50} shell. Color code: purple, Ag; red, O; gray, C; green, F.

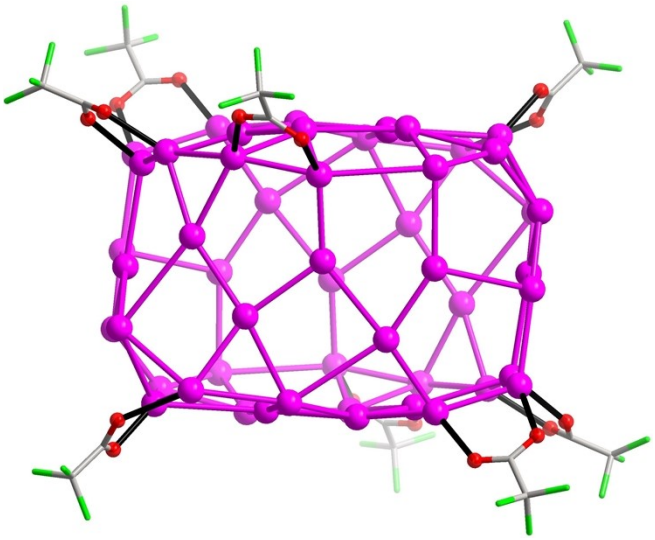

Figure S9: The picture of the crystal (**Ag50**) used for SCXRD analysis.

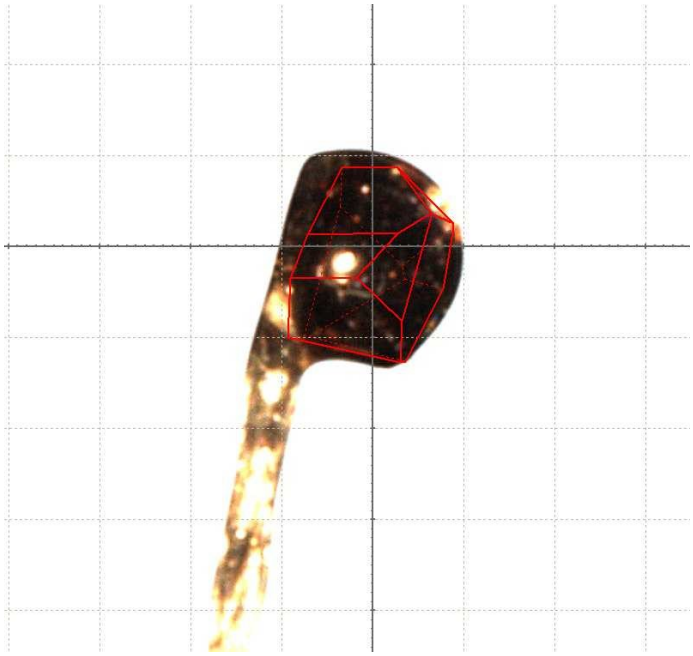

Figure S10: The surface of **Ag50** calculated via 3V Volume Assessor program[11] by rolling a virtual probe (5.0 Å) on the surface viewed along six different orientations.

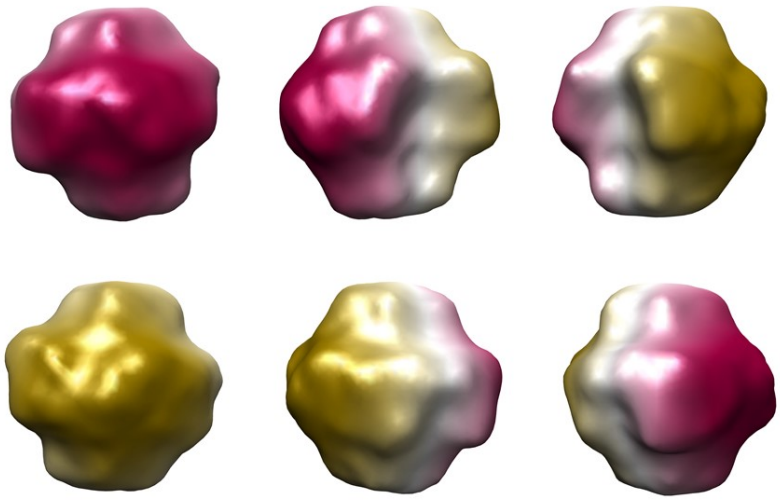

Figure S11: The photograph of the fresh crystals of **Ag50** under an optical microscope.

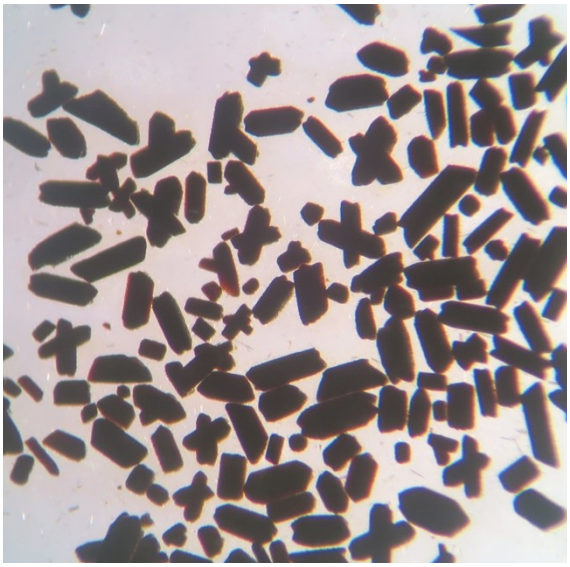

Table S1: The summary of polyoxymolybdate-, polyoxytungstate- and polyoxovanadate-templated silver clusters.

Formula	Structure	Ref.
α-Mo_5O_{18}@Ag_{38}(^{t}BuS)$_{18}$(PhCOO)$_{14}$·2CH_2Cl_2	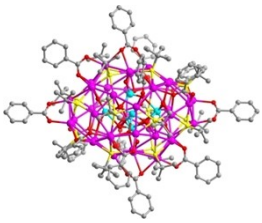	12
Mo_6O_{22}@Ag_{44}(^{i}PrS)$_{20}$(PhCOO)$_{16}$(CH_3CN)$_2$·2CH_3CN	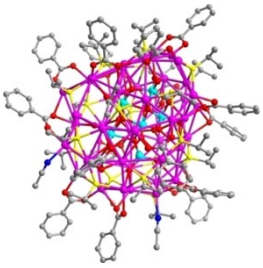	13
Mo_8O_{28}@Ag_{50}(^{i}PrS)$_{24}$(PhCOO)$_{18}$(CH_3CN)$_2$·4CH_3CN	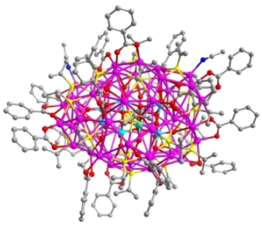	
Mo_6O_{22}@Ag_{46}(^{t}BuPhS)$_{32}$(dppm)$_4$(CH_3CN)$_8$·6CF_3SO_3	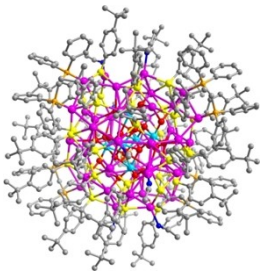	14
Mo_6O_{22}@$Ag_{58}S_2$(^{t}BuPhS)$_{36}$(CF_3COO)$_{10}$(H_2O)$_8$	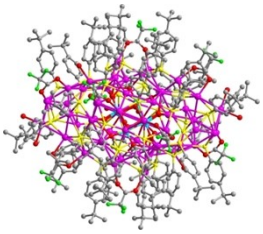	15
(Mo_6O_{22})$_2$@Ag_{60}(^{t}BuC≡C)$_{38}$(CF_3SO_3)$_4$	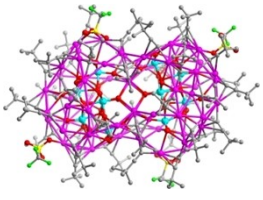	16

$(Mo_6O_{22})_2$@$Ag_{76}(MeOPhS)_{28}(dppm)_8(MoO_4)_{16}(H_2O)_8\cdot 8CH_3OH\cdot 4CH_3CN$	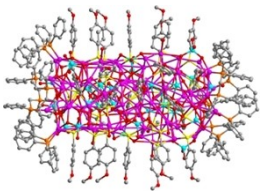	17
Mo_7O_{24}@$Ag_{41}(^iPrS)_{19}(Tos)_{16}(CH_3OH)_4\cdot 4CH_3OH$	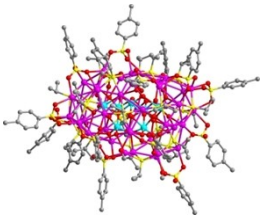	18
$(^nBu_4N)_{1.5}[Mo_5O_{18}$@$Ag_{36}(^iPrS)_{18}(Tos)_{13.5}(CH_3CN)]\cdot 1.5CH_3CN$	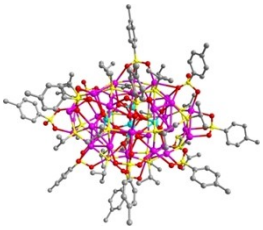	
Mo_8O_{28}@Ag_{48}(*p*-$MePhS)_{24}(CF_3COO)_{14}(H_2O)_4(DMF)_2\cdot 2CF_3COO$	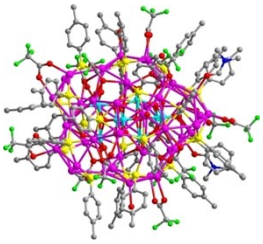	19
α-Mo_5O_{18}@$Ag_{36}(^iPrS)_{18}(PhSO_3)_{12}(DMF)_6$	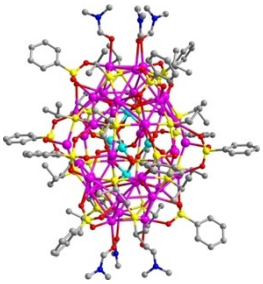	20
$\{(^nBu_4NH)[\beta\text{-}Mo_5O_{18}$@$Ag_{36}(^iBuS)_{18}(PhSO_3)_{13}(CH_3OH)]\}_n$	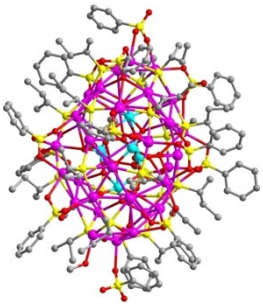	

$[Mo_2O_8@Ag_{30}(^{i}BuS)_{15}(PhSO_3)_{11}(CH_3OH)_2(H_2O)\cdot H_2O]_2$	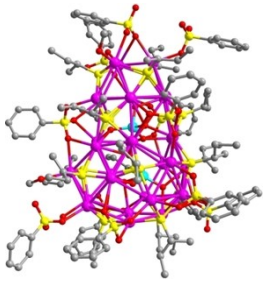	
$[Mo_4O_{14}(SO_4)]_2@Ag_{73}S_4(PhSO_3)_{17}(^{i}BuS)_{30}(SO_4)_3(H_2O)_4\cdot 2H_2O$	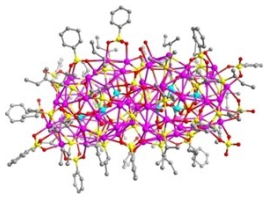	
$Ag_{10}@(Mo_7O_{26})_2@Ag_{70}(MoO_4)_2(CyS)_{36}(CF_3SO_3)_{16}(DMF)_6\cdot 2DMF\cdot 4^{n}PrOH$	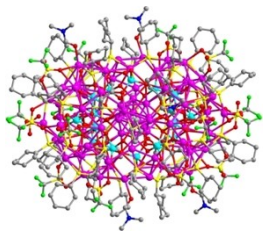	21
$Ag_{10}@(Mo_7O_{26})_2@Ag_{70}(MoO_4)_2(^{i}PrS)_{36}(CF_3SO_3)_{16}(DMF)_6$	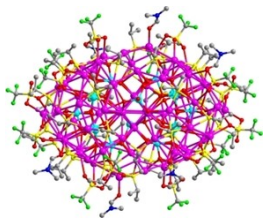	
$Mo_{20}O_{66}@Ag_{62}(^{t}BuS)_{40}(Mo_6O_{19})_3(CH_3CN)_2\cdot 4CF_3SO_3$	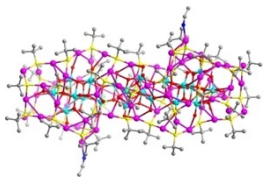	22
$Mn^{III}Mn^{IV}_2Mo_{14}O_{56}@Ag_{64}(^{t}BuC{\equiv}C)_{38}(CF_3COO)_8(OH)\cdot 10CH_3CN\cdot 2H_2O$	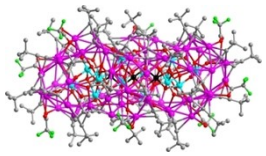	23
$Mo_6O_{22}@Ag_{40}(^{t}BuC{\equiv}C)_{20}(CF_3COO)_{12}(CH_3OH)_2$	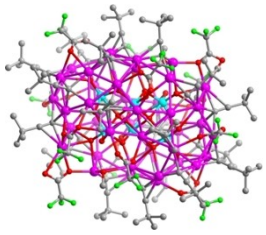	24

$[Mo_6O_{19}@Ag_{44}(EtS)_{24}(SCl_4)_3]_n$	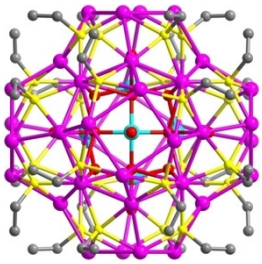	25
$Cu_3Mo_8O_{32}@Ag_{55}(CyS)_{43}(CH_3O)(CF_3COO)\cdot 3H_2O$	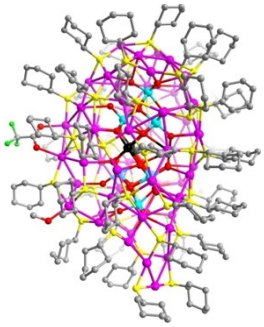	26
$K(H_2O)HP_5W_{30}O_{110}@Ag_{43}(^tBuC{\equiv}C)_{29}(CN)(CH_3CN)(H_2O)\cdot 4CH_3CN$	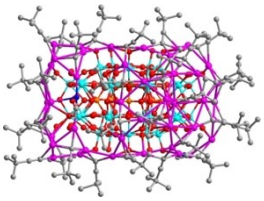	27
$(PW_9O_{34})_2@Ag_{67}(p\text{-}FPhS)_{36}(DMAc)_2(CF_3COO)_6\cdot 7CF_3COO\cdot xDMAc$	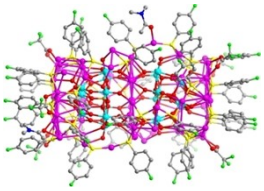	28
$(PW_9O_{34})_2@Ag_{70}(^tBuC{\equiv}C)_{44}(H_2O)_2\cdot 8BF_4\cdot 2(BMIm)BF_4\cdot 3H_2O$	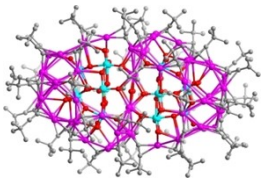	29
$(SO_4)_2(W_5O_{19})_2@Ag_{90}(^tBuPhS)_{44}(PhCOO)_{24}(DMF)_2(H_2O)_2\cdot 2PhCOO$	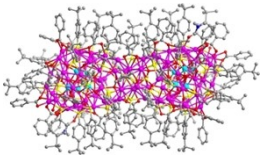	30
$W_6O_{21}@Ag_{34}(^tBuS)_{26}(CF_3COO)\cdot CF_3COO\cdot Et_3N\cdot 20CH_3OH$	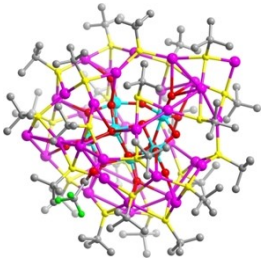	31

$Ag_{10}@(W_7O_{26})_2@Ag_{74}S_2(^{i}PrS)_{40}(^{n}PrCOO)_{18}\cdot 2CH_3OH$	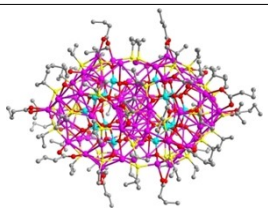	32
$Ag_{10}@(W_7O_{26})_2@Ag_{74}S_2(^{i}PrS)_{40}(PhCOO)_{18}$	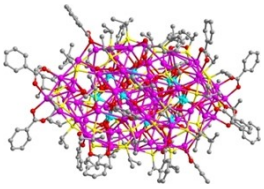	
$Ho(W_5O_{18})_2@Ag_{42}(^{t}BuC{\equiv}C)_{28}Cl_4\cdot OH$	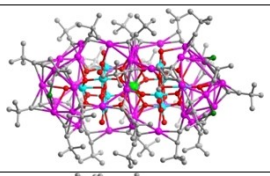	33
$Eu(W_5O_{18})_2@Ag_{42}(^{t}BuC{\equiv}C)_{28}Cl_4\cdot OH\cdot H_2O$	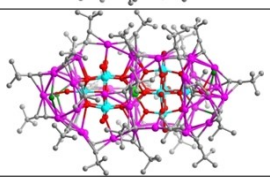	34
$(EuW_{10}O_{36})_2@Ag_{72}(^{t}BuC{\equiv}C)_{48}Cl_2\cdot 4BF_4$	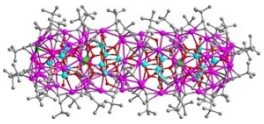	35
$\alpha\text{-}SiW_{10}O_{37}@Ag_{41}(^{t}BuC{\equiv}C)_{27}(CH_3CN)_3\cdot\beta\text{-}SiW_{12}O_{40}\cdot H_2O\cdot 4CH_3CN$	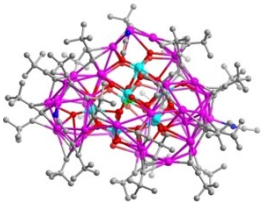	36
$SiW_9O_{34}@Ag_{34}Cu_6(^{t}BuC{\equiv}C)_{18}(^{t}BuPO_3)_9(CH_3CN)_2(H_2O)\cdot 2CH_3CN$	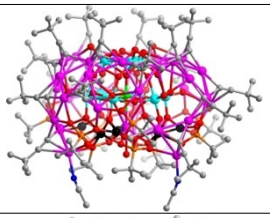	37
$SiW_9O_{34}@Ag_{37}Cu_6(^{t}BuC{\equiv}C)_{18}(^{t}BuPO_3)_9(CH_3CN)_6\cdot 0.5SiW_{12}O_{40}\cdot OH$	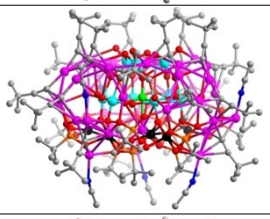	
$(WO_6)(SiW_9O_{34})@Ag_{51}(^{t}BuC{\equiv}C)_{27}(^{n}BuPO_3)_3(CH_3COO)_3(CH_3CN)_3\cdot 0.5H_8SiW_{12}O_{40}\cdot BF_4$	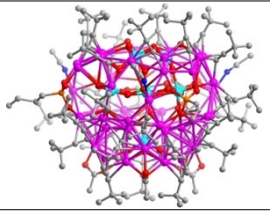	

$W_{10}O_{32}@Ag_{44}(^{t}BuS)_{24}(CF_3COO)_8(CF_3COO)_6\cdot 6H_2O$	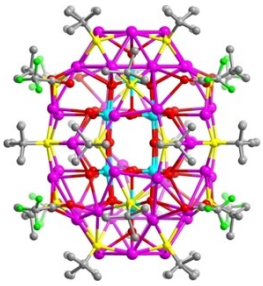	38
$(CO_3)(CoW_{12}O_{40})_2@Ag_{42}(^{t}BuC{\equiv}C)_{27}(CH_3CN)_2$	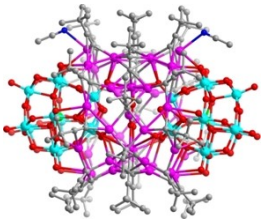	39
$PW_9O_{34}@Ag_{51}(^{i}PrS)_{25}(CF_3COO)_{17}(DMF)_3(CH_3OH)_3$	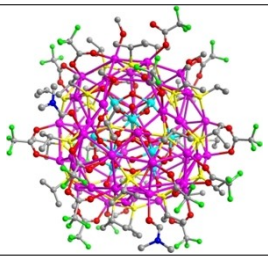	40
$\{[(PW_9O_{34})_2@Ag_{72}S(^{i}PrS)_{41}(CF_3COO)_8(bipy)_{5.5}(CH_3OH)(H_2O)]\cdot 3CF_3COO\}_n$	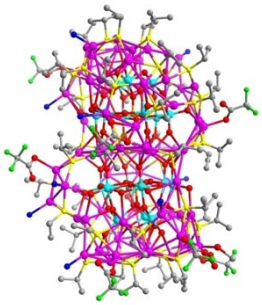	
$\{[(PW_9O_{34})_2@Ag_{72}S(^{i}PrS)_{42}(CF_3COO)_7(pi\text{-}bipy)_{4.5}(CH_3OH)]\cdot 3CF_3COO\}_n$		
$(P_2W_{15}Nb_3O_{62})@Ag_{25}(^{t}BuC{\equiv}C)_{16}(CH_3CN)_4$	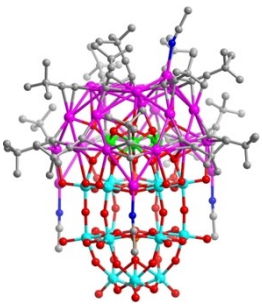	41
$(^{n}Bu_4N)[Ag_{42}(CO_3)(SiW_9Nb_3O_{40})_2@(^{t}BuC{\equiv}C)_{27}]\cdot 5CH_3CN$	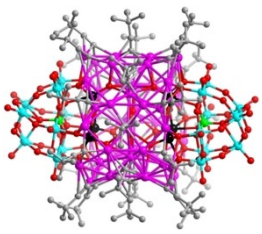	42

$[(Et)_4N]_3\{[(O_2)V_2O_6]_2@Ag_{36}(^tBuC{\equiv}C)_{12}[(^tBuPO_3)_4V_4O_8]_2(^tBuPO_3)_2(NO_3)_7(2\text{-}ClPy)(DMF)\}$	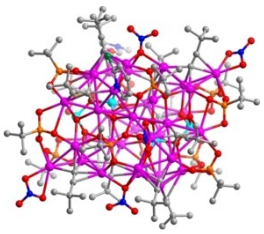	43
$[(Et)_4N]_2\{[(O_2)V_2O_6]_2Cl@Ag_{36}(^tBuC{\equiv}C)_{11}[(^tBuPO_3)_4V_4O_8]_2[(^tBuPO_3)_2(VO_2)](^tBuPO_3)_2(^tBuPO_3H)(DMF)(NO_3)_2(Et_2O)(H_2O)_3\}\cdot 2DMF\cdot 2Et_2O\cdot 4H_2O$	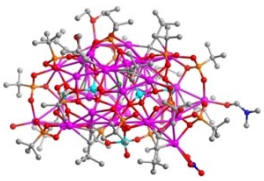	
$\{[(O_2)V_2O_6]_3@Ag_{43}(PhC{\equiv}C)_{19}[(^tBuPO_3)_4V_4O_8]_3(DMF)_6\}\cdot 5DMF\cdot 2H_2O$	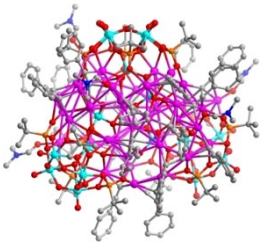	44
$[V_{10}O_{28}@Ag_{44}(EtS)_{20}(PhSO_3)_{18}(H_2O)_2]_n$	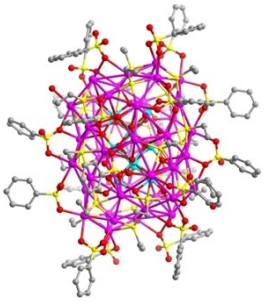	25
$[V_{10}O_{28}@Ag_{46}(EtS)_{23}(PhSO_3)_{15}(CO_3)]_n$	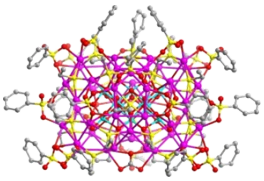	
$V^V{}_{10}V^{IV}{}_2O_{34}@Ag_{30}(^tBuS)_{20}\cdot 10CH_3OH$	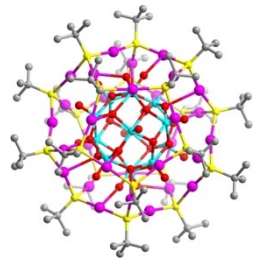	45
$V^V{}_{10}V^{IV}{}_2O_{34}@Ag_{30}(^tBuS)_{20}\cdot 8CH_3OH$		
$V^V{}_{10}V^{IV}{}_2O_{34}@Ag_{30}(^tBuS)_{20}\cdot 7CH_3OH$	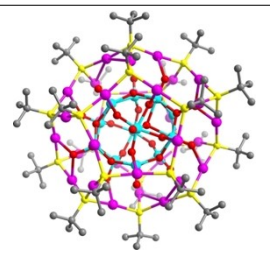	

$V_{10}O_{28}@Ag_{40}(^{t}BuC{\equiv}C)_{22}(CF_3COO)_{12}\cdot 4CH_3OH$	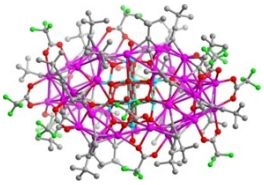	24
$V_2O_7@Ag_{24}(^{t}BuC{\equiv}C)_{14}(CF_3COO)_6\cdot 2CH_3OH$	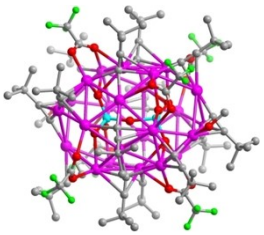	
$[Bz(Et)_3N]_8[(Et)_4N]_2[(V_2O_7)_2@Ag_{44}(^{t}BuC{\equiv}C)_{14}@(V_{32}O_{96})]$	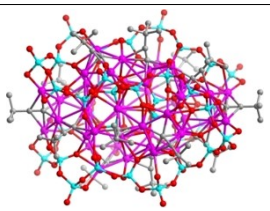	46
$V_2O_7@Ag_{24}(^{t}BuC{\equiv}C)_{14}(hfac)_6$	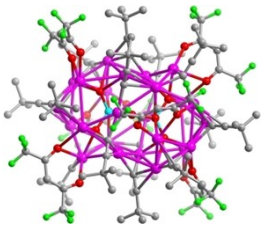	47
$V_2O_7@Ag_{40}(^{t}BuC{\equiv}C)_{22}(^{t}BuPO_3)_4(hfac)_4(CF_3COO)_2(H_2O)_2$	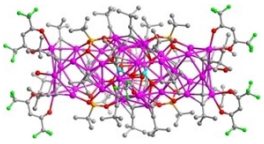	
Note: dppm = bis-(diphenylphosphino)methane; DMF = N,N-dimethylformamide; DMAc = N,N-dimethylacetamide; hfac = hexafluoroacetylacetone; Cy = cyclohexyl; ^{i}Pr = iso-propyl; ^{n}Pr = normal-propyl; ^{t}Bu = tert-butyl; ^{i}Bu = iso-butyl; Tos = *p*-toluenesulfonate; bipy = 4,4'-bipyridine; pi-bipy = 1,4-bis(4-pyridinylmethyl)piperazine; BMIm = 1-butyl-3-methylimidazolium; Bz = benzyl; py = pyridine.		

Table S2: BVS calculations for the V atoms of **Ag50**.

Atom	V^{III}	V^{IV}	V^{V}
V1	4.421	4.808	<u>5.061</u>
V2	4.320	4.697	<u>4.945</u>
V3	4.389	4.772	<u>5.024</u>
V4	4.316	4.694	<u>4.941</u>
V5	4.338	4.717	<u>4.965</u>
The underlined value is the one closest to the charge for which it was calculated. The oxidation state can be taken as the integer nearest to the underlined value.			

Table S3: The formulae of the key species detected in positive-ion mode ESI-MS of **Ag50** dissolved in MeOH-CH_2Cl_2.

Peak	Species	Exp. *m/z*	Sim. *m/z*
1a	$[V_{10}O_{28}@Ag_{46}(^t\text{BuPhS})_{27}(CF_3COO)_9(H_2O)_2]^{4+}$	2858.254	2858.202
1b	$[V_{10}O_{28}@Ag_{46}(^t\text{BuPhS})_{28}(CF_3COO)_8(H_2O)_2]^{4+}$	2871.774	2871.724
1c	$[V_{10}O_{28}@Ag_{46}(^t\text{BuPhS})_{29}(CF_3COO)_7(H_2O)_2]^{4+}$	2884.788	2884.746
1d	$[V_{10}O_{28}@Ag_{46}(^t\text{BuPhS})_{30}(CF_3COO)_6(H_2O)_2]^{4+}$	2898.249	2898.268
1e	$[V_{10}O_{28}@Ag_{47}(^t\text{BuPhS})_{28}(CF_3COO)_9(H_2O)_2]^{4+}$	2926.994	2926.947
1f	$[V_{10}O_{28}@Ag_{47}(^t\text{BuPhS})_{29}(CF_3COO)_8(H_2O)_2]^{4+}$	2939.515	2939.469
1g	$[V_{10}O_{28}@Ag_{47}(^t\text{BuPhS})_{30}(CF_3COO)_7(H_2O)_2]^{4+}$	2953.261	2953.241
1h	$[V_{10}O_{28}@Ag_{47}(^t\text{BuPhS})_{31}(CF_3COO)_6(H_2O)_2]^{4+}$	2966.234	2966.263
1i	$[V_{10}O_{28}@Ag_{48}(^t\text{BuPhS})_{28}(CF_3COO)_{10}(H_2O)_2]^{4+}$	2982.219	2982.169
1j	$[V_{10}O_{28}@Ag_{48}(^t\text{BuPhS})_{29}(CF_3COO)_9(H_2O)_2]^{4+}$	2995.233	2995.191
1k	$[V_{10}O_{28}@Ag_{48}(^t\text{BuPhS})_{30}(CF_3COO)_8(H_2O)_2]^{4+}$	3008.499	3008.463
1l	$[V_{10}O_{28}@Ag_{48}(^t\text{BuPhS})_{31}(CF_3COO)_7(H_2O)_2]^{4+}$	3021.722	3021.736
1m	$[V_{10}O_{28}@Ag_{49}(^t\text{BuPhS})_{29}(CF_3COO)_{10}(H_2O)_2]^{4+}$	3050.702	3050.664
1n	$[V_{10}O_{28}@Ag_{49}(^t\text{BuPhS})_{30}(CF_3COO)_9(H_2O)_2]^{4+}$	3063.471	3063.436
1o	$[V_{10}O_{28}@Ag_{49}(^t\text{BuPhS})_{31}(CF_3COO)_8(H_2O)_2]^{4+}$	3076.481	3076.458
1p	$[V_{10}O_{28}@Ag_{50}(^t\text{BuPhS})_{29}(CF_3COO)_{11}(H_2O)_2]^{4+}$	3105.184	3105.136
1q	$[V_{10}O_{28}@Ag_{50}(^t\text{BuPhS})_{30}(CF_3COO)_{10}(H_2O)_2]^{4+}$	3118.692	3118.659
1r	$[V_{10}O_{28}@Ag_{50}(^t\text{BuPhS})_{31}(CF_3COO)_9(H_2O)_2]^{4+}$	3131.958	3131.931

Table S4: Crystal data and structure refinements for **Ag50**.

Compound	**Ag50**
Empirical formula	$C_{398}H_{542}Ag_{50}F_{36}N_{18}O_{74}S_{32}V_{10}$
Formula weight	14375.28
Temperature/K	99.9(3)
Crystal system	monoclinic
Space group	$P2_1/n$
a/Å	25.6844(3)
b/Å	27.1429(2)
c/Å	36.5460(4)
α/°	90
β/°	91.7718(9)
γ/°	90
Volume/Å^3	25465.9(5)
Z	2
ρ_{calc}g/cm^3	1.875
μ/mm^{-1}	18.328
F(000)	14128.0
Radiation	Cu Kα (λ = 1.54184)
Reflections collected	145654
Independent reflections	44825[Rint = 0.0657, Rsigma = 0.0596]
Data/parameters	44825/2756
Goodness-of-fit on F^2	1.029
Final R indexes [I>=2σ (I)]	R_1= 0.1448, wR_2= 0.3506
Final R indexes [all data]	R_1= 0.1575, wR_2= 0.3593
Largest diff. peak/hole/eÅ^{-3}	3.77/-3.43

Table S5: Selected bond distances (Å) and bond angles (°) for **Ag50**.

Ag50			
Ag1—Ag2	2.923(11)	Ag16—S2	2.497(4)
Ag1—Ag3	2.936(5)	Ag16—S10	2.539(5)
Ag1—Ag16^{i}	3.210(3)	Ag16—S16^{i}	2.737(8)
Ag1—O10^{i}	2.555(11)	Ag17—Ag18	3.086(3)
Ag1—S13	2.345(6)	Ag17—Ag23^{i}	2.927(2)
Ag1—S16	2.413(6)	Ag17—S2	2.443(4)
Ag2—Ag3	2.915(16)	Ag17—S6	2.431(5)
Ag2—Ag7	3.325(12)	Ag18—Ag19	2.866(3)
Ag2—S11	2.678(14)	Ag18—O16	2.38(2)
Ag2—S13	2.889(14)	Ag18—S4^{i}	2.568(5)
Ag3—S1	2.348(16)	Ag18—S6	2.555(6)
Ag3—S16	2.669(9)	Ag18—S8	2.694(6)
Ag4—Ag5	2.805(11)	Ag19—O15	2.24(2)
Ag4—Ag20^{i}	2.715(6)	Ag19—S4^{i}	2.900(5)
Ag4—S9^{i}	2.602(8)	Ag19—S8	2.905(6)
Ag5—Ag19	3.172(8)	Ag19—S15	2.474(6)
Ag5—Ag20^{i}	3.026(6)	Ag20—O13	2.474(11)
Ag5—S15	2.12(1)	Ag20—S5	2.861(5)
Ag6—O21	2.14(3)	Ag20—S9	2.456(5)
Ag6—S9^{i}	2.74(3)	Ag20—S15^{i}	2.495(6)
Ag6—S10^{i}	2.89(3)	Ag21—Ag22	2.865(3)
Ag6—S16	2.622(13)	Ag21—Ag23	3.323(2)
Ag7—Ag8	2.858(4)	Ag21—O20	2.390(18)
Ag7—O9^{i}	2.522(10)	Ag21—S4	2.552(5)
Ag7—S1	2.584(12)	Ag21—S5	2.617(5)
Ag7—S8	2.576(5)	Ag21—S15^{i}	2.817(7)
Ag7—S11	2.467(6)	Ag22—Ag24	2.984(3)
Ag8—Ag9	3.373(3)	Ag22—O19	2.413(18)
Ag8—Ag18	2.949(3)	Ag22—S5	2.484(5)
Ag8—O5^{i}	2.547(10)	Ag22—S7	2.434(6)
Ag8—S3	2.382(5)	Ag23—O7	2.34(1)
Ag8—S8	2.435(5)	Ag23—S2^{i}	2.658(5)
Ag9—Ag10	3.006(3)	Ag23—S4	2.456(5)
Ag9—Ag11	3.148(3)	Ag23—S7	2.687(5)
Ag9—S3	2.564(5)	Ag24—Ag25	3.051(2)
Ag9—S11	2.548(6)	Ag24—O24	2.300(18)
Ag9—S14	2.665(6)	Ag24—S7	2.489(5)
Ag10—Ag24	2.954(3)	Ag24—S14	2.455(7)
Ag10—Ag25	3.025(2)	Ag25—O6	2.444(11)
Ag10—O23	2.267(19)	Ag25—S2^{i}	2.714(4)

Ag10—S11	2.773(6)	Ag25—S7	2.533(5)
Ag10—S13	2.683(6)	Ag25—S13	2.447(6)
Ag10—S14	2.763(7)	Ag13—S12	2.306(9)
Ag11—Ag12	3.119(2)	Ag14—Ag15	3.261(3)
Ag11—Ag14	2.985(3)	Ag14—O17	2.43(2)
Ag11—Ag15	3.233(3)	Ag14—S10	2.430(6)
Ag11—O14	2.463(10)	Ag14—S12	2.518(6)
Ag11—S3	2.461(5)	Ag15—Ag16	3.322(3)
Ag11—S12	2.428(6)	Ag15—Ag17	2.964(3)
Ag12—Ag22	3.036(3)	Ag15—S3	2.544(5)
Ag12—Ag24	3.072(2)	Ag15—S6	2.661(6)
Ag12—S5	2.524(5)	Ag15—S10	2.422(7)
Ag12—S12	2.787(7)	Ag16—Ag17	3.228(3)
Ag12—S14	2.556(6)	Ag16—O11	2.552(10)
Ag12—O14	2.79(1)	Ag13—O25	2.43(3)
Ag13—S9	2.547(9)	Ag13—Ag14	3.207(8)
S13—Ag1—O10^{i}	78.4(3)	O6—Ag25—S13	118.5(3)
S13—Ag1—S16	157.73(19)	S7—Ag25—S2^{i}	94.13(15)
S16—Ag1—O10^{i}	123.9(3)	S13—Ag25—S2^{i}	111.29(18)
S11—Ag2—S13	89.5(4)	S13—Ag25—S7	140.65(18)
S1—Ag3—S16	131.4(4)	S9—Ag20—S15^{i}	143.4(2)
O21—Ag6—S9^{i}	103.3(9)	S15^{i}—Ag20—S5	99.5(2)
O21—Ag6—S10^{i}	99.1(15)	O20—Ag21—S4	102.7(6)
O21—Ag6—S16	114.7(9)	O20—Ag21—S5	102.7(7)
S9^{i}—Ag6—S10^{i}	137.7(3)	O20—Ag21—S15^{i}	102.0(7)
S16—Ag6—S9^{i}	116.8(13)	S4—Ag21—S5	143.90(16)
S16—Ag6—S10^{i}	84.4(5)	S4—Ag21—S15^{i}	101.52(17)
O9^{i}—Ag7—S1	87.1(4)	S5—Ag21—S15^{i}	97.81(17)
O9^{i}—Ag7—S8	95.6(3)	O19—Ag22—S5	104.1(6)
S8—Ag7—S1	109.6(4)	O19—Ag22—S7	113.4(6)
S11—Ag7—O9^{i}	107.5(3)	S7—Ag22—S5	138.74(17)
S11—Ag7—S1	110.6(4)	O7—Ag23—S2^{i}	101.6(3)
S11—Ag7—S8	134.2(2)	O7—Ag23—S4	105.8(3)
S3—Ag8—O5^{i}	94.5(3)	O7—Ag23—S7	106.1(3)
S3—Ag8—S8	149.86(19)	S2^{i}—Ag23—S7	91.96(15)
S8—Ag8—O5^{i}	115.5(3)	S4—Ag23—S2^{i}	130.14(15)
S3—Ag9—S14	110.4(2)	S4—Ag23—S7	118.32(17)
S11—Ag9—S3	119.78(19)	O24—Ag24—S7	108.1(6)
S11—Ag9—S14	111.0(2)	O24—Ag24—S14	107.8(7)
O23—Ag10—S11	119.7(7)	S14—Ag24—S7	141.07(16)
O23—Ag10—S13	99.3(6)	O6—Ag25—S2^{i}	96.4(3)
O23—Ag10—S14	100.3(6)	O6—Ag25—S7	86.2(3)
S13—Ag10—S11	91.85(2)	S2—Ag16—O11	104.8(3)

S13—Ag10—S14	146.28(18)	S2—Ag16—S10	136.56(17)
S14—Ag10—S11	101.81(18)	S2—Ag16—S16^{i}	118.96(17)
O14—Ag11—S3	110.4(3)	S10—Ag16—O11	113.7(3)
S12—Ag11—O14	98.8(3)	S10—Ag16—S16^{i}	89.27(19)
S12—Ag11—S3	150.63(18)	S6—Ag17—S2	155.45(17)
S5—Ag12—S12	102.05(18)	O16—Ag18—S4^{i}	98.3(7)
S5—Ag12—S14	158.5(2)	O16—Ag18—S6	100.0(7)
S14—Ag12—S12	98.9(2)	O16—Ag18—S8	97.4(7)
O25—Ag13—S9	106.5(10)	S4^{i}—Ag18—S8	118.26(17)
S12—Ag13—O25	111.9(10)	S6—Ag18—S4^{i}	122.66(17)
S12—Ag13—S9	141.2(3)	S6—Ag18—S8	112.49(16)
O17—Ag14—S12	101.6(6)	O15—Ag19—S4^{i}	105.4(7)
S10—Ag14—O17	113.9(5)	O15—Ag19—S8	97.5(8)
S10—Ag14—S12	141.76(18)	O15—Ag19—S15	139.8(8)
S3—Ag15—S6	86.11(16)	S4^{i}—Ag19—S8	102.18(15)
S10—Ag15—S3	141.99(19)	S15—Ag19—S4^{i}	101.2(2)
S10—Ag15—S6	131.90(18)	S15—Ag19—S8	105.7(2)
O11—Ag16—S16^{i}	77.4(3)	O13—Ag20—S5	80.2(3)
S9—Ag20—S5	104.82(18)	O13—Ag20—S15^{i}	112.8(3)
S9—Ag20—O13	98.3(3)	O13—Ag20—S15^{i}	112.8(3)

Reference:

1. Tang, K. L.; Xie, X. J.; Zhao, L.; Zhang, Y. H.; Jin, X. L. Synthesis and crystal structure of $\{[HNEt_3]_{2n}[Ag_8Ag_{4/2}(SC_6H_4tBu\text{-}4)_{12}]_n \cdot nC_2H_5OH\}$ and its reaction product with CS_2. *Eur. J. Inorg. Chem.* **2004**, 2004, 78-85.
2. Iki, N.; Kabuto, C.; Fukushima, T.; Kumagai, H.; Takeya, H.; Miyanari, S.; Miyashi, T.; Miyano, S. Synthesis of *p-tert*-butylthiacalix[4]arene and its inclusion property. *Tetrahedron* **2000**, 56, 1437-1443.
3. Rigaku Oxford Diffraction. *CrysAlis^{Pro} software system, version 1.171.40.84a,* Rigaku Corporation: Oxford, UK, **2018**.
4. Chaki, N. K.; Mandal, S.; Reber, A. C.; Qian, M.; Saavedra, H. M.; Weiss, P. S.; Khanna, S. N.; Sen, A. Controlling band gap energies in cluster-assembled ionic solids through internal electric fields. *ACS Nano* **2010**, 4, 5813-5818.
5. Sheng, K.; Wang, R.; Tang, X. D.; Jagodič, M.; Jaglicič, Z.; Pang, L. X.; Dou, J. M.; Gao, Z. Y.; Feng, H. Y.; Tung, C. H.; Sun, D. A carbonate-templated decanuclear Mn nanocage with two different silsesquioxane ligands. *Inorg. Chem.* **2021**, 60, 14866-14871.
6. Clark, R. C.; Reid, J. S. The analytical calculation of absorption in multifaceted crystals. *Acta Crystallogr.* **1995**, A51, 887-897.
7. Sheldrick, G. M. *SHELXT*-Integrated space-group and crystal-structure determination. *Acta Crystallogr.* **2015**, A71, 3-8.
8. Sheldrick, G. M. Crystal structure refinement with SHELXL. *Acta Crystallogr.* **2015**, C71, 3-8.
9. Dolomanov, O. V.; Bourhis, L. J.; Gildea, R. J.; Howard, J. A. K.; Puschmann, H. OLEX2: a complete structure solution, refinement and analysis program. *J. Appl. Crystallogr.* **2009**, 42, 339-341.
10. Spek, A. L. Structure validation in chemical crystallography. *Acta Crystallogr.* **2009**, D65, 148-155.
11. Voss, N. R.; Gerstein, M. 3V: cavity, channel and cleft volume calculator and extractor. *Nucleic. Acids. Res.* **2010**, 38, W555-W562.
12. Su, Y. M.; Liu, W.; Wang, Z.; Wang, S. A.; Li, Y. A.; Yu, F.; Zhao, Q. Q.; Wang, X. P.; Tung, C. H.; Sun, D. Benzoate-induced high-nuclearity silver thiolate clusters. *Chem. Eur. J.* **2018**, 24, 4967-4972.

13. Wang, Z.; Su, H. F.; Tung, C. H.; Sun, D.; Zheng, L. S. Deciphering synergetic core-shell transformation from [Mo_6O_{22}@Ag_{44}] to [Mo_8O_{28}@Ag_{50}]. *Nat. Commun.* **2018**, 4407.
14. Li, X. Y.; Wang, Z.; Su, H. F.; Feng, S.; Kurmoo, M.; Tung, C. H.; Sun, D.; Zheng, L. S. Anion-templated nanosized silver clusters protected by mixed thiolate and diphosphine. *Nanoscale* **2017**, 9, 3601-3608.
15. Li, X. Y.; Tan, Y. Z.; Yu, K.; Wang, X. P.; Zhao, Y. Q.; Sun, D.; Zheng, L. S. Atom-precise polyoxometalate-Ag_2S core-shell nanoparticles. *Chem. Asian. J.* **2015**, 10, 1295-1298.
16. Qiao, J.; Shi, K.; Wang, Q. M. A giant silver alkynyl cage with sixty silver(I) ions clustered around polyoxometalate templates. *Angew. Chem. Int. Ed.* **2010**, 49, 1765-1767.
17. Liu, J. W.; Feng, L.; Su, H. F.; Wang, Z.; Zhao, Q. Q.; Wang, X. P.; Tung, C. H.; Sun, D.; Zheng, L. S. Anisotropic assembly of Ag_{52} and Ag_{76} nanoclusters. *J. Am. Chem. Soc.* **2018**, 140, 1600-1603.
18. Wang, Z.; Su, H. F.; Kurmoo, M.; Tung, C. H.; Sun, D.; Zheng, L. S. Trapping an octahedral Ag_6 kernel in a seven-fold symmetric Ag_{56} nanowheel. *Nat. Commun.* **2018**, 9, 2094.
19. Wang, Z.; Zhuo, H. Y.; Hu, A. Y.; Su, H. F.; Zhao, Q. Q.; Wang, X. P.; Tung, C. H.; Sun, D. Self‐assembly of a novel Ag_{48} cluster encapsulating an unprecedented $[Mo_8O_{28}]^{8-}$ anion template. *Isr. J. Chem.* **2019**, 59, 280-285.
20. Wang, Z.; Su, H. F.; Wang, X. P.; Zhao, Q. Q.; Tung, C. H.; Sun, D.; Zheng, L. S. Johnson solids: anion-templated silver thiolate clusters capped by sulfonate. *Chem. Eur. J.* **2018**, 24, 1640-1650.
21. Su, Y. M.; Wang, Z.; Zhuang, G. L.; Zhao, Q. Q.; Wang, X. P.; Tung, C. H.; Sun, D. Unusual fcc-structured Ag_{10} kernels trapped in Ag_{70} nanoclusters. *Chem. Sci.* **2019**, 10, 564-568.
22. Huang, R. W.; Xu, Q. Q.; Lu, H. L.; Guo, X. K.; Zang, S. Q.; Gao, G. G.; Tang, M. S.; Mak, T. C. W. Self-assembly of an unprecedented polyoxomolybdate anion $[Mo_{20}O_{66}]^{12-}$ in a giant peanut-like 62-core silver-thiolate nanocluster. *Nanoscale* **2015**, 7, 7151-7154.
23. Wang, J. Y.; Liu, K. G.; Guan, Z. J.; Nan, Z. A.; Lin, Y. M.; Wang, Q. M. $[Mn^{III}Mn^{IV}_2Mo_{14}O_{56}]^{17-}$: a mixed-valence meso-polyoxometalate anion encapsulated by a 64-nuclearity silver cluster. *Inorg. Chem.* **2016**, 55, 6833-6835.
24. Gao, G. G.; Cheng, P. S.; Mak, T. C. W. Acid-induced surface functionalization of polyoxometalate by enclosure in a polyhedral silver-alkynyl cage. *J. Am. Chem. Soc.* **2009**, 131,

18257-18259.

25. Wang, Z.; Sun, Y. M.; Qu, Q. P.; Liang, Y. X.; Wang, X. P.; Liu, Q. Y.; Kurmoo, M.; Su, H. F.; Tung, C. H.; Sun, D. Enclosing classical polyoxometallates in silver nanoclusters. *Nanoscale* **2019**, 11, 10927-10931.
26. Gao, J. P.; Qi, Z. K.; Zhang, F. Q.; Zhang, X. M. *In situ* insertion of copper to form heteroanionic D_{3h}-symmetric $[Cu_3Mo_8O_{32}]^{10-}$ for a templated Ag_{55} nanocluster. *Nanoscale* **2022**, 14, 4469-4473.
27. Zhang, S. S.; Chen, J. Y.; Li, K.; Yuan, J. D.; Su, H. F.; Wang, Z.; Kurmoo, M.; Li, Y. Z.; Gao, Z. Y.; Tung, C. H.; Sun, D.; Zheng, L. S. Janus cluster: asymmetric coverage of a Ag_{43} cluster on the symmetric preyssler P_5W_{30} polyoxometalate. *Chem. Mater.* **2021**, 33, 9708-9714.
28. Yan, B. J.; Du, X. S.; Huang, R. W.; Yang, J. S.; Wang, Z. Y.; Zang, S. Q.; Mak, T. C. W. Self-assembly of a stable silver thiolate nanocluster encapsulating a lacunary keggin phosphotungstate anion. *Inorg. Chem.* **2018**, 57, 4828-4832.
29. Jiang, Z. G.; Shi, K.; Lin, Y. M.; Wang, Q. M. $[Ag_{70}(PW_9O_{34})_2(^tBuC{\equiv}C)_{44}(H_2O)_2]^{8+}$: ionothermal synthesis of a silver cluster encapsulating lacunary polyoxometalate ions. *Chem. Commun.* **2014**, 50, 2353-2355.
30. Liu, J. W.; Su, H. F.; Wang, Z.; Li, Y. A.; Zhao, Q. Q.; Wang, X. P.; Tung, C. H.; Sun, D.; Zheng, L. S. A giant 90-nucleus silver cluster templated by hetero-anions. *Chem. Commun.* **2018**, 54, 4461-4464.
31. Zhou, K.; Qin, C.; Li, H. B.; Yan, L. K.; Wang, X. L.; Shan, G. G.; Su, Z. M.; Xu, C.; Wang, X. L. Assembly of a luminescent core-shell nanocluster featuring a $Ag_{34}S_{26}$ shell and a $W_6O_{21}^{6-}$ polyoxoanion core. *Chem. Commun.* **2012**, 48, 5844-5846.
32. Wang, Z.; Sun, H. T.; Kurmoo, M.; Liu, Q. Y.; Zhuang, G. L.; Zhao, Q. Q.; Wang, X. P.; Tung, C. H.; Sun, D. Carboxylic acid stimulated silver shell isomerism in a triple core-shell Ag_{84} nanocluster. *Chem. Sci.* **2019**, 10, 4862-4867.
33. Li, Y. Y.; Gao, F.; Beves, J. E.; Li, Y. Z.; Zuo, J. L. A giant metallo-supramolecular cage encapsulating a single-molecule magnet. *Chem. Commun.* **2013**, 49, 3658-3660.
34. Song, C. Y.; Chai, D. F.; Zhang, R. R.; Liu, H.; Qiu, Y. F.; Guo, H. D.; Gao, G. G. A silver-alkynyl cluster encapsulating a fluorescent polyoxometalate core: enhanced emission and fluorescence modulation. *Dalton. Trans.* **2015**, 44, 3997-4002.

35. Zhang, S. S.; Su, H. F.; Wang, Z.; Wang, X. P.; Chen, W. X.; Zhao, Q. Q.; Tung, C. H.; Sun, D.; Zheng, L. S. Elimination-fusion self-assembly of a nanometer-scale 72-Nucleus silver cluster caging a pair of $[EuW_{10}O_{36}]^{9-}$ polyoxometalates. *Chem. Eur. J.* **2018**, 24, 1998-2003.

36. Liu, K. G.; Liu, X. Y.; Guan, Z. J.; Shi, K.; Lin, Y. M.; Wang, Q. M. The transformation of polyoxometalates in the formation of intercluster compound $[Ag_{41}(\alpha\text{-}SiW_{10}O_{37})(^{t}BuC{\equiv}C)_{27}(CH_3CN)_3][\beta\text{-}SiW_{12}O_{40}]$. *Chem. Commun.* **2016**, 52, 3801-3804.

37. Duan, G. X.; Xie, Y. P.; Jin, J. L.; Bao, L. P.; Lu, X.; Mak, T. C. W. High-nuclearity heterometallic *tert*-butylethynide clusters assembled with *tert*-butylphosphonate. *Chem. Eur. J.* **2018**, 24, 6762-6768.

38. Yu, J. Q.; Xue, C. H.; Zhou, K.; Fang, Y.; Ji, J. Y.; Chen, B. K.; Bi, Y. F. Trapping a $[W_{10}O_{32}]^{6-}$ decatungstate anion in an Ag_{44} nanowheel. *Chem. Asian J.* **2022**, 17, e202200072.

39. Gruber, F.; Jansen, M. $\{[Ag_{42}(CO_3)(C{\equiv}C\textit{t}Bu)_{27}(CH_3CN)_2][CoW_{12}O_{40}]_2\}[BF_4]$: an intercluster sandwich compound. *Angew. Chem. Int. Ed.* **2010**, 49, 4924-4926.

40. Wang, Z.; Zhu, Y. J.; Li, Y. Z.; Zhuang, G. L.; Song, K. P.; Gao, Z. Y.; Dou, J. M.; Kurmoo, M.; Tung, C. H.; Sun, D. Nuclearity enlargement from $[PW_9O_{34}@Ag_{51}]$ to $[(PW_9O_{34})_2@Ag_{72}]$ and 2D and 3D network formation driven by bipyridines. *Nat. Commun.* **2022**, 13, 1802.

41. Kurasawa, M.; Arisaka, F.; Ozeki, T. Asymmetrically fused polyoxometalate-silver alkynide composite cluster. *Inorg. Chem.* **2015**, 54, 1650-1654.

42. Tamari, S.; Ono, K.; Hashimoto, M.; Ozeki, T. Control over the preference for binding sites of polyoxometalates to silver ethynide clusters by surface charge modification. *Dalton. Trans.* **2015**, 44, 19056-19058.

43. Xie, Y. P.; Mak, T. C. W. High-nuclearity silver ethynide clusters assembled with phosphonate and metavanadate precursors. *Angew. Chem. Int. Ed.* **2012**, 51, 8783-8786.

44. Xie, Y. P.; Mak, T. C. W. Silver(I)-ethynide clusters constructed with phosphonate-functionized polyoxovanadates. *J. Am. Chem. Soc.* **2011**, 133, 3760-3763.

45. Liu, H.; Song, C. Y.; Huang, R. W.; Zhang, Y.; Xu, H.; Li, M. J.; Zang, S. Q.; Gao, G. G. Acid-base-triggered structural transformation of a polyoxometalate core inside a dodecahedrane-like silver thiolate shell. *Angew. Chem. Int. Ed.* **2016**, 55, 3699-3703.

46. Xie, Y. P.; Mak, T. C. W. A pyrovanadate-templated silver(I)-ethynide cluster circumscribed by macrocyclic polyoxovanadate(V). *Chem. Commun.* **2012**, 48, 1123-1125.

47. Jin, J. L.; Shen, Y. L.; Xie, Y. P.; Lu, X. Silver ethynide clusters constructed with fluorinated β-diketonate ligands. *CrystEngComm* **2018**, 20, 2036-2042.